Universality of a two-dimensional Ising ferromagnetic fluid near the second-order magnetic phase transition

W. Korneta
Faculty of Physics, Technical University, Malczewskiego 29, 26-600 Radom, Poland
(Received 3 May 2001; published 25 September 2001)

The critical behavior of a two-dimensional (2D) system of hard disks, each disk bearing an Ising spin and interacting via Ising-like interactions, is studied near the second-order phase transition from the paramagnetic-to-ferromagnetic fluid phase by Monte Carlo simulations combined with a finite-size scaling analysis and a single histogram technique. The critical line is located and values of critical exponents along this line are determined. The continuous variation of the Binder's reduced fourth-order cumulant at the critical point and of the critical exponent ν with disk density is observed and a linear relation between these quantities is found. Ratios of critical exponents γ/ν and β/ν are found to be the same as those in the 2D Ising lattice model at all fluid densities. A statistical analysis of Voronoi diagrams generated for typical particle configurations along the critical line is performed. The variation of parameters characterizing Voronoi diagrams at the critical point with density is compared to the variation of critical exponents with density.

DOI: 10.1103/PhysRevE.64.041109 PACS number(s): 64.60.Fr, 75.40.Mg, 75.40.Cx, 75.50.Mm

I. INTRODUCTION

The simplest model of a fluid is a two-dimensional (2D) hard-disk system. This model has been of concern for a number of decades [1,2], because it exhibits the freezing transition and because of its use as the reference system for many perturbation theories of fluids. A two-dimensional hard-disk system has been extensively studied by computer simulation methods: the Monte Carlo (MC) method, which evaluates ensemble averages, and by the molecular-dynamics (MD) method, in which dynamical equations of motion for particles are solved. Both methods are fundamental in theoretical studies of fluid properties. They give excellent agreement with experiment provided that sufficiently realistic potential-energy functions are used [1]. It is widely accepted that both MC and MD supply ''experimental'' data and any approximate theory of liquids can be tested against these ''experimental'' data. The MC method was proposed by Metropolis *et al.* [3] in 1953, and applied to get an equation of state for 224 hard disks in two dimensions. The obtained results did not indicate any phase transition. Alder and Wainwright [4] applied the MD method to study a 2D system of 870 hard disks and demonstrated very clearly the coexistance of solid and fluid phases at high densities, what is typical of the first-order phase transition. Hoover and Alder [5] showed that equations of state for a 2D hard-disk system obtained by the MC and MD methods are identical. A major conclusion following from computer simulations is that 2D hard-disk systems show the phase transition from fluid to solid phases at high densities. This transition is a weak first-order transition with a narrow gap between the coexisting densities and low metastability barier between the solid and the disordered fluid. The earliest approximate theories of fluids were the cell or free-volume theories [1]. They were based on the idea that molecules in a liquid for most of the time are confined to cells formed by their neighbors. In the cell model, the communal entropy arising from communal sharing of the volume, and due to the presence of density fluctuations, is neglected. In order to evaluate how bad the cell theories are and suggest the way to modify them, Hoover and Ree [6] made MC simulations of a 2D hard-disk single-occupancy cell model, i.e., the model with one disk per cell. The authors showed that in the fluid phase, this model reproduces the hard-disk equation of state surprisingly well. Among other approximate theoretical methods, the density-functional theory was particularly useful in the study of fluid properties. The solid near melting is considered as a perturbation on the fluid, and the order parameters characterizing the fluid-solid phase transition are the amplitudes of density waves [7–10] . Results for 2D hard disks obtained from density-functional calculations and computer simulations were compared by Zeng and Oxtoby [10]. They are very close. There are also approximate theories of a 2D classical hard-disk fluid based on the correlation functions between disks. Lado [11] and Chae, Ree, and Ree [12] compared results from MC simulations and from four theories: the Born-Green-Yvon (BGY), the Percus-Yevick (PY), the convolution-hypernetted-chain (CHNC), and the pressure-consistent (PC) theory. These approximate theories allow one to obtain the pair radial distribution function by numerical integrations and iterations of integral equations. The PY theory was found to provide the best results consistent with MC simulations.

In 1968, Busch and Guentherodt [13] reported the first experimental evidence for ferromagnetism in the liquid state. They investigated liquid alloys with transition metals that in the solid phase are amorphous ferromagnets. The paper stimulated both experimental and theoretical studies of magnetic liquids. The theoretical models of magnetic liquids are based on the existing classical models of liquids that fairly well describe the microscopic and macroscopic static and dynamic properties of liquids [1]. In magnetic liquids, there are additional magnetic degrees of freedom that are on an equal footing with other degrees of freedom. The interplay between spatial and magnetic degrees of freedom leads to complex phase diagrams of magnetic fluids with the first- and second-order transitions as well as tricritical and triple points both in the quantum [14–16] and classical [17–20]

limits. In this paper, we consider a model for ferromagnetic fluid consisting of hard-core particles with a classical spin degrees of freedom. Frankel and Thompson [17] first examined the thermodynamic properties of this model for the interaction potential between spins of Kac type $\epsilon^D K(\epsilon|\mathbf{r}|)$ in the long-range limit. The free energy in this case is a combination of the classical van der Waals and Curie-Weiss expressions. The qualitative features of this model and its phase diagram are dimension independent. Frankel and Thompson suggested the application of the model to amorphous ferromagnets, dilute magnetic alloys, silicon spin glasses, and with suitable modifications, to liquid crystals. Hemmer and Imbro [18] considered a system of hard-core particles interacting with weak long-ranged exchange interactions in addition to the spin-independent isotropic attractive forces. Applying the effective-field theory, they derived two coupled equations of state for the average magnetization and pressure. The equations were used to obtain phase diagrams for the 1D system with Ising spins and the 3D system with Heisenberg spins. Depending on the ratio of the integrated strengths of the magnetic and nonmagnetic interactions, topologically different phase diagrams occur. The same 3D system of hard-core particles with Heisenberg spins was also studied within the mean-field (MF) and the modified mean-field (MMF) approximations of the density functional theory (DFT) [20]. The different types of phase diagrams obtained by Hemmer and Imbro were qualitatively reproduced, and for a system without isotropic interactions a remarkable good agreement with MC simulations [21] was noticed. Lomba and coworkers [19] considered the 3D system of hard spheres with embedded Heisenberg spins whose coupling constant is given by Yukawa ferromagnetic interaction. They carried out Gibbs' ensemble Monte Carlo simulations to investigate the liquid-gas coexistence curve. They found that the system lacks a tricritical point and the line of Curie points ends at a critical endpoint on the gas side of the gas-liquid coexistence curve. This disagreed with predictions of both the DFT [20] and the effective-field theory [18]. The contradiction was discussed in Ref. [20].

The critical properties of ferromagnetic fluids have been much less studied than their phase diagrams. The configurational disorder in magnetic fluids is brought about by thermal motions, so they are classified as annealed disordered magnetic systems. According to the universality arguments, magnetic fluids with short-ranged interactions should exhibit the same critical properties as dilute localized magnets. A fixed particle density in a fluid correspond to a fixed degree of dilution in the lattice. Let us first briefly review the results obtained so far for ferromagnetic lattice models with configurational disorder that are the most related with this paper. The comprehensive review of basic static properties of dilute localized magnets with both quenched and annealed, bond and site disorder, is given in Ref. [22]. The main conclusion following from the study of the second-order magnetic phase transition in these systems is that a small amount of disorder should not change the critical behavior and values of critical exponents if the specific heat exponent α of the pure system is negative. On the contrary, when $\alpha>0$, critical exponents take renormalized values [22]. Above a certain amount of disorder one expects the critical behavior to change in both cases. It has, however, not yet been established definitively, whether critical exponents vary continuously with the amount of disorder, or they adopt new universal values corresponding to the existence of a new random fixed point. Moreover, it is generally thought that scaling relations between critical exponents are always preserved. First, MC simulations for the simple cubic Ising model with quenched site dilution failed to get any difference of critical exponents from pure critical exponents [23]. Because the exponent α of the pure system is positive [22], the critical behavior was expected to change. Marro, Labarta, and Tejada [24] performed MC analysis in larger systems and revealed a line of fixed points. They obtained critical exponents varying continuously with dilution. Kim and Patrascioiu [25] studied the 2D randomly site-diluted Ising model on the square lattice by MC simulations. They observed a continuous increase of critical exponents of the magnetic susceptibility γ and of the correlation length ν with dilution, whereas the ratio $\gamma/\nu = 1.75$ remained as those in the pure system [22]. They also noticed that Binder's reduced fourth-order cumulant [26–28] at the critical point is increasing with dilution. Kühn [29] studied the same model using the real-space renormalization group (RSRG) method and a method that combines a grand ensemble approach to disordered systems with phenomenological renormalization. His results are in complete qualitative and quantitative accord with MC simulations. Derrida and coworkers [30] considered the Binder's cumulant in the 2D quenched bond-diluted Ising lattice model in stripe geometry applying MC simulations. They noticed the variation of the cumulant with the amount of disorder and suggested also that critical exponents should vary continuously. They made the conjecture that the value of the cumulant at the critical point characterizes universality class. The exponent α is zero for the pure 2D Ising lattice model, so the disorder is marginally irrelevant in this case, and it is unclear if any change of critical exponents should be expected. The investigations of a randomly spin-diluted 2D Ising lattice model suggest weak universality in this case in the sense that exponents γ, β, and ν increase with dilution, while γ/ν and β/ν are constant and the same as those in the pure 2D Ising lattice model.

The critical properties of ferromagnetic fluids have been studied since 1996, and the results obtained so far are inconclusive [21,31,32]. All authors combined MC simulations with a finite-size scaling analysis and with single and/or multiple histogram techniques. The finite-size scaling (FSS) method allows one to extract the proper critical behavior from the rounded singularities produced by the finite size of the simulated systems [26–28]. The single [33] and multiple [34] histogram techniques proposed by Ferrenberg and Swendsen greatly enhanced the accuracy and improved the efficiency of MC simulations in the critical region. The single histogram technique allows one to obtain complete thermodynamic information over the entire scaling region near a phase transition from a single MC run. The multiple histogram technique is an optimized method for combining data from several MC runs both to increase the total accuracy of the results and to obtain information over a wide range of

parameter values. Ferrenberg and Swendsen tested both techniques against the exact solution of the 2D Ising lattice model and they have got an excellent agreement. MC simulations with a finite-size scaling analysis and histogram techniques have also been used to investigate 3D classical Ising [35] and Heisenberg [36] simple cubic models for which the exact results are as yet unknown. The critical properties have been determined with a precision comparable to that obtained with renormalization-group and series-expansion techniques. Nowadays, this method is the most frequently used to obtain highly accurate estimates for the location of phase transition and values of critical exponents in systems with unknown or partially known behavior. Nijmeijer and Weis [21] considered a 3D fluid of hard spheres that carry a Heisenberg spin and interact via Yukawa-type exchange coupling. Their estimates for exponent ratios β/ν and γ/ν are the same for all fluid densities and satisfy the scaling relation $2\beta/\nu+\gamma/\nu=D$ with $D=3$. The Binder's reduced fourth-order cumulant at the critical point and the value of the correlation length critical exponent ν increased at lower fluid densities. Wilding and Nielaba [31] studied the tricritical point properties of a 2D system of hard disks each of which has Ising spin interacting via a distance-dependent spin coupling of the square well type. They located the tricritical point and determined exponents of the three relevant scaling fields controlling the behavior of the system in the vicinity of this point. Ferreira and Korneta [32] considered the same model assuming the Yukawa form of the exchange coupling between spins. They described critical properties of the model at low-disk density near the second-order phase transition from the paramagnetic to the ferromagnetic fluid. The obtained critical exponent ν is much higher than in the 2D Ising lattice model, whereas ratios of critical exponents β/ν and γ/ν are the same as those in the 2D Ising lattice model.

In this paper, we concentrate on the critical behavior of the 2D hard-disk Ising fluid near the second-order magnetic phase transition in the range of densities higher than the tricritical point density and lower than the freezing density. The aim of the paper is to answer several questions following from the summary given above, e.g., is the weak universality observed in dilute localized magnets also appropriate to characterize critical properties of magnetic fluids? Does the value of Binder's cumulant at the critical point follow changes of critical exponents with fluid density? Is the dependence of critical properties in the Ising and Heisenberg fluids on the density qualitatively correlated? How bad are the approximate cell or mean-field approximations (MFA) theories in predicting the location of the critical line? Is the Voronoi diagram useful in the description of structural changes in the magnetic fluid at the critical point with density? We performed MC simulations, and the finite-size scaling analysis in the same way as it was done by Ferreira and Korneta [32], but in larger systems to reduce corrections to the scaling. We applied the single histogram technique to the simulation data in order to get the thermodynamic information over the entire scaling regime. The model and MC simulation details are described in Sec. II. The location of the critical line determined from MC simulations and obtained within the cell model and MFA theory is given in Sec. III. The critical exponents of the spin-correlation length, the magnetization and magnetic susceptibility are considered in Sec. IV. The characterization of structural changes of the fluid along the critical line based on the analysis of Voronoi diagrams is presented in Sec. V. Finally, all obtained results are summarized in conclusions.

II. THE MODEL AND SIMULATION DETAILS

The model to be considered is a simplified representation for a 2D fluid of particles with two internal magnetic states. Particles represented by hard disks of diameter σ have translational degrees of freedom, and each particle has an internal Ising spin ($S=\pm 1$). Usually, the most important contribution to intermolecular potential energy is from pair interactions between spins and other multibody interactions are negligible. In this paper, we assume the Ising-like interaction between spins favoring their ferromagnetic alignment, with the distance-dependent exchange coupling $J(r/\sigma)$. There are two approximations of the effective exchange coupling between spins used in theoretical studies of magnetic fluids: the crude square-well approximation [14–16,31] and the Yukawa-type smooth approximation [19,21,32]. We assume the Yukawa-type coupling between spins $J(r/\sigma)$ in the form

$$J\left(\frac{r}{\sigma}\right) \Big/ k_B T = -K\frac{\sigma}{r}\exp\left[-z\sigma\left(\frac{r}{\sigma}-1\right)\right], \qquad (1)$$

where k_B is the Boltzmann's constant, T is the temperature, $z\sigma$ is the screening parameter, and $K>0$ expresses the ratio of exchange energy to thermal energy. The quantity $1/z\sigma$ is a measure for the range of exchange interactions. All MC simulations in this paper were performed for $z\sigma=1$. This model was studied for one fluid density in Ref. [32].

At high temperatures, only the hard-core repulsion remains and the system is paramagnetic for all densities. At high densities, there is a temperature-independent hard-disk first-order freezing transition. As the temperature is reduced, the system undergoes a second-order phase transition from a paramagnetic hexagonal solid to ferromagnetic hexagonal solid at high densities and from a paramagnetic to ferromagnetic fluid at intermediate densities. In the ferromagnetic phase, the freezing density decreases with decreasing the temperature due to greater stability of the solid phase arising from magnetic interactions. The line of critical points separating the paramagnetic fluid phase from the ferromagnetic fluid phase, called the critical line or the Curie line, terminates at the tricritical point [31]. The particle density varies continuously across this line. At low densities, there is a strong tendency to clustering in the system. Following the critical line to lower densities, the density fluctuations grow, and at the tricritical point, the critical line merges into the gas-liquid coexistance region. This region corresponds to the so-called condensation-ordering first-order phase transition [20], where order-disorder and gas-liquid first-order phase transitions are coupled. In this region, a low-density paramagnetic gas and a high-density ferromagnetic liquid coexist. The condensation-ordering first-order transition meets at the triple point of the freezing first-order phase transition. At

the triple point, ferromagnetic fluid coexists with ferromagnetic hexagonal solid. For temperatures below the triple point temperature, there is a first-order phase transition between paramagnetic gas and ferromagnetic hexagonal solid.

MC simulations we performed in the canonical (N,V,T) ensemble in which the particle number N, the total volume V, and the temperature T are fixed [1,37]. The square simulation box with periodic boundary conditions was assumed, so the surface effects were avoided. In simulations, we used the nearest-image distance convention [37] and we truncated the pair interaction at a distance 6.3246σ. In order to avoid the calculation of distances between particles that are too far apart to interact, the simulation box was partitioned into cells and the method of linked lists of neighbors [37] was used. We applied a regular Metropolis scheme [3] to sample positions of disks and the algorithm described by Lomba *et al.* [19] to sample spin degrees of freedom. At one Monte Carlo step (MCS) we attempted to move a randomly selected particle to a new position and rotate its spin. In all simulations, the total number of Monte Carlo steps per particle (MCS/N) was the same and equal 2×10^6. During the simulation, the total spin and energy of the system were stored to a file every 10 MCS/N. The disks were initially placed at random for low densities or on the square lattice for densities greater than half of the close-packed density. All runs started from random spin directions. The approach of the system to equilibrium in all cases was fairly rapid and discarding the first 10^4 MCS/N ensured that all subsequent configurations were generated for the system at equilibrium. The maximum position displacement of a particle was adjusted during the first discarded MCS, so that to get the acceptance ratio of trial moves around 50% [37]. Instead of performing simulations for various areas of the simulation box and fixed-particle diameter, we always considered the equivalent problem of keeping the box length $L=1$ fixed and changing, the particle diameter. This is recommended in Ref. [3,37] to speed up simulations. The stored data we binned to evaluate both the systematic and statistical errors that arise from finite length of MC runs [38]. These errors are similar as in Ref. [32] and we do not plot them here.

III. LOCATION OF THE CRITICAL LINE

The density of hard-disk fluid is usually expressed by two dimensionless quantities: the number density $\rho=N\sigma^2/L^2$ [8,10,11,14–16,19,21,31,32] and the packing fraction $\eta=N\pi\sigma^2/(4L^2)=\pi\rho/4$ [9], where L is the simulation box length. In hard-core systems, the maximum allowed density is the close-packed density. The close packing of hard disks corresponds to their arrangement in a trigonal lattice [3] with densities $\rho_{cp}=2/\sqrt{3}\simeq1.1547$ and $\eta_{cp}=\pi/(2\sqrt{3})\simeq0.9069$. The most suitable quantity to characterize the state of the hard-core disk system is the reduced packing fraction $\eta/\eta_{cp}=\rho/\rho_{cp}$ often used in the equations of state [3–6,12]. This ratio we use in all plots. At high densities, disks become sufficiently localized [4] and the fluid crystallizes. The point of marginal mechanical stability where the solid starts to form, and the point of marginal thermodynamic stability where the solid ceases to be metastable relative to the fluid of the same density, were determined by both numerical methods and approximate theories. The results are listed in the Table in Ref. [10]. The obtained densities of the fluid at marginal mechanical stability are in the range between $\eta/\eta_{cp}=0.694$ [8] and $\eta/\eta_{cp}=0.786$ [9]. We performed MC simulations at the density $\eta/\eta_{cp}=0.693$ ($\rho=0.8$) and at lower densities given in Tables I and II, i.e., in the range where the fluid phase is stable. For densities lower than $\eta/\eta_{cp}=0.346$ ($\rho=0.4$) the system approaches the tricritical point that follows from the analysis of Voronoi diagrams discussed in the Sec. V.

TABLE I. The values of coupling parameter K for which MC simulations were performed. N denotes the number of particles in the system and ρ is the number density.

ρ	$N=1296$	$N=1156$	$N=1024$	$N=900$	$N=784$	$N=676$
0.8	0.198	0.198	0.198	0.197	0.198	
0.7	0.238	0.239	0.239	0.239	0.238	0.239
0.6	0.296	0.298	0.296	0.296	0.299	0.296
0.6	0.290	0.290	0.290	0.290	0.290	0.290
0.55	0.337	0.338	0.338	0.338	0.338	0.338
0.55	0.320	0.320	0.320	0.320	0.320	0.320
0.5	0.389	0.389	0.389	0.386	0.386	0.389
0.5	0.370	0.370	0.370	0.370	0.370	0.370
0.45	0.460	0.460	0.460	0.450	0.455	0.460
0.45	0.430	0.425	0.431	0.430	0.420	0.415
0.4	0.546	0.545	0.545	0.545	0.546	

Let us define by $M=\Sigma_i S_i/N$ the average value of particle spin in the system. The central quantity used to precisely locate the critical point both in localized magnets and magnetic fluids is the Binder's reduced fourth-order cumulant U defined as [21,26–28,32,35,36]:

$$U=1-\frac{\langle M^4\rangle}{3\langle M^2\rangle^2}, \tag{2}$$

where $\langle\ldots\rangle$ denotes the canonical ensemble average [3]. The variation of U with the simulation box size for a fixed value of K can be interpreted as the renormalization-group flow diagram [26,27]. Upon increasing the box size, the cu-

TABLE II. The critical value of the Binder's cumulant U_c, the critical coupling K_c, and the estimated critical exponent ν of the correlation length for different Ising ferromagnetic fluid densities. ρ denotes the number density and η/η_{cp} is the reduced packing fraction.

ρ	η/η_{cp}	K_c	U_c	ν
0.8	0.6928	0.1989	0.6050	1.00
0.7	0.6062	0.2400	0.6065	1.02
0.6	0.5196	0.2989	0.6120	1.09
0.55	0.4763	0.3386	0.6160	1.14
0.5	0.4330	0.3886	0.6210	1.20
0.45	0.3897	0.4540	0.6260	1.27
0.4	0.3464	0.5430	0.6320	1.35

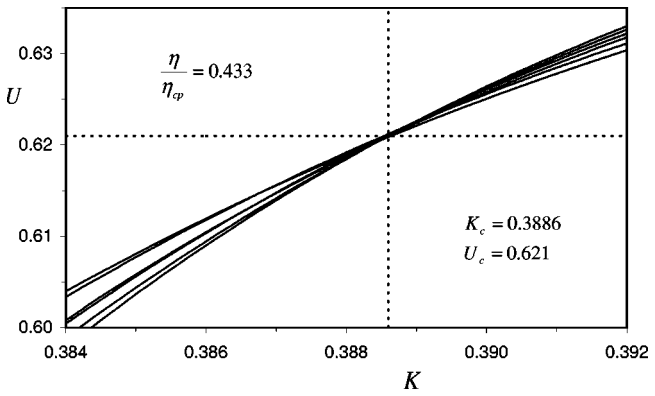

FIG. 1. Plot of the Binder's cumulant U versus the coupling K in systems composed of 1296, 1156, 1024, 900, 784, and 676 disks for the reduced packing fraction $\eta/\eta_{cp}=0.433$. The curves result from a single histogram technique. The slope of the curves increases with the number of disks in the system. The critical point is determined by dotted lines. The estimated values of the critical coupling K_c and of the cumulant at the critical point U_c are indicated.

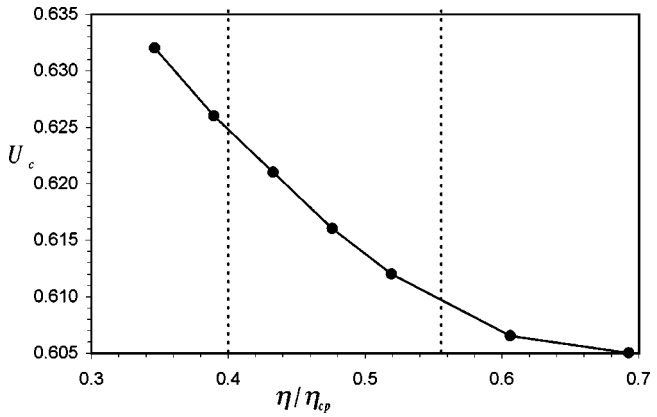

FIG. 2. The Binder's cumulant at the critical point U_c versus the reduced packing fraction η/η_{cp}. The dots represent values of U_c obtained from MC simulations via cumulant crossing method shown in Fig. 1. The curve is drawn to guide the eye. The dotted lines determine characteristic packing fractions described in Ref. [3] and in the text.

mulant tends to $U=0$ in the paramagnetic phase and to $U=2/3$ in the ferromagnetic phase. At the critical point $K=K_c$, the cumulant U approaches the nontrivial fixed-point value. The similar properties have also the higher-order cumulants. In the vicinity of the critical point, the probability distribution function of M satisfies the finite-size scaling hypothesis. The form of the distribution, however, strongly depends both on the boundary conditions used and on the shape of the simulation box [26,27,30]. The probability distribution function of M at the critical point and its cumulants are thus universal only in this restricted sense. In practice, the critical point is located by performing a single MC simulation in the critical region and applying histogram techniques [33,34] to get the dependence of the cumulant U on K over the entire scaling regime. At the critical point, the curves $U=f(K)$ intersect in a common intersection point independent of the size of the simulation box. We first performed short MC runs to get a crude approximation of K_c for all considered densities. In Table I we give the number of particles in the system, densities, and values of the coupling parameter K for which we performed long MC simulations.

Applying a single histogram technique and locating the intersection point of cumulants, we determined the value of the critical coupling K_c and the value of the cumulant at the critical point U_c for different densities of the ferromagnetic fluid. The intersection of curves $U=f(K)$ for $\rho=0.5$ and different system sizes is shown in Fig. 1. The obtained values of K_c and U_c are given in Table II. In Fig. 2, we show the dependence of U_c on the reduced packing fraction. The Binder's cumulant at the critical point varies continuously with the density. Metropolis and coworkers [3] determined numerically by MC simulations the equation of state for a 2D system of noninteracting hard disks. Their results coincide with the results of the free-volume theory for $\eta/\eta_{cp}>0.556$ and with the five-term virial expansion for $\eta/\eta_{cp}<0.4$. In Fig. 2 one can notice the change in the dependence $U_c=f(\eta/\eta_{cp})$ for $\eta/\eta_{cp}\simeq 0.56$. For fluid densities where deviations from the free-volume theory become large, U_c quickly increases with decreasing fluid density. The same qualitatively dependence of the Binder's cumulant on the density was found in the Heisenberg fluid [21] and in the 2D site-diluted Ising lattice model [25]. The value of the Binder's cumulant at the critical point obtained in the 2D Ising lattice model assuming periodic boundary conditions is $U_c=0.611$ [39].

The critical line resulting from our MC simulations is shown in Fig. 3. The circular data points on this line can serve as ''experimental'' data points to be fitted by the critical line obtained within approximate theories. In models of ferromagnetic fluids, the approximation can be applied to the configurational degrees of freedom and/or to spin degrees of

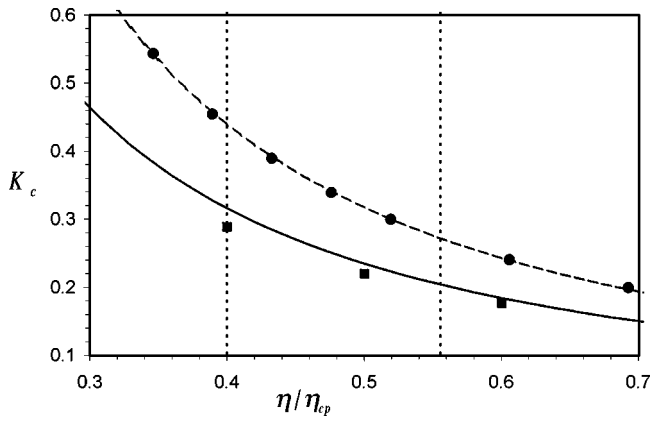

FIG. 3. The dependence of the critical coupling K_c on the reduced packing fraction η/η_{cp}. The dots represent critical points obtained from MC simulations via cumulant crossing method shown in Fig. 1. The squares result from the approximate theory of ferromagnetic Ising fluid described in Ref. [42] and in the text. The solid and dashed curves are critical lines in the cell model for the screening parameter $z\sigma=1$ and $z\sigma=\sqrt{2}$, respectively. The dotted lines determine characteristic packing fractions described in Ref. [3] and in the text.

freedom. The earliest approximate theories of liquids were the cell theories [1]. In the simplest uncorrelated cell models, it is assumed that particles are constrained to occupy individual cells and correlations between particles in different cells are ignored. In fact, one also exploits this idea in MC simulations, but a cell (simulation box) contains several hundred particles instead of one. The single-occupancy cell model can thus be considered as a rough first approximation of a fluid. In ferromagnetic fluid, each particle moves in the field of the others, and this field may be replaced by a suitable average field. Lennard-Jones and Devonshire [40] proposed the uncorrelated cell model for a system of interacting hard-core particles and determined the equation of state of a fluid at moderate densities. They assumed that the average field in which any one particle moves is the field produced by other particles localized at their most probable positions, the centers of their cells. In the model of Lennard-Jones and Devonshire, the central particle moves randomly in the symmetrical available region of radius $d-\sigma$ (d is the average distance between nearest neighbors) about the center of its cell, while positions of other particles are fixed. The maximum amplitude of motion can be interpreted as the mean radius of the free volume in the free-volume theories [41]. We applied the same approximation to our system of hard disks with Ising spins assuming that disks are contained in regular hexagonal cells. The choice of hexagonal cells is motivated by the fact that for a 2D hard-disk system, the most probable number of neighbors is six for all densities [2]. We calculated numerically the effective magnetic field acting on a central particle, and applying the mean-field Weiss approximation, we determined the critical line shown as the solid line in Fig. 3. The shorter exchange coupling makes it harder for the spins to order, and hence, yields a lower critical temperature. For the screening parameter $z\sigma=\sqrt{2}$, i.e., when the range of exchange interactions is shortened, the critical line shifts to higher values of K and fits well to MC simulation data. The Lennard-Jones and Devonshire cell model provided the basis for other systematic theories of fluids [6,40], e.g., the correlated-cell theories or the cluster theories [1]. Although for $z\sigma=\sqrt{2}$ the cell model correctly predicts here both the shape and position of the critical line, it does not imply that the cell structure exists in real fluids.

The approximate theory of a ferromagnetic fluid that has been the most frequently used until now to predict the location of the critical line and the tricritical point is the theory in which spins are treated in the mean-field approximation and spatial correlations between particles are like in classical liquids [15,21,42]. It is based on the assumption that the magnetic transition is determined mainly by the magnetic interaction strength and both spin correlations and the temperature do not effect the fluid structure. The effective magnetic-field h acting on one spin can thus be approximated by

$$h=-2\pi\rho M\int J\left(\frac{r}{\sigma}\right)g\left(\frac{r}{\sigma}\right)\frac{r}{\sigma}d\left(\frac{r}{\sigma}\right), \tag{3}$$

where $g(r/\sigma)$ denotes the positional radial pair-distribution function. It expresses the local number density of disks at a distance r/σ from a disk at the origin divided by ρ. $g(r/\sigma)$ approaches one as the distance becomes large. The most accurate correlations of particles in fluids are determined in computer-generated ''experiments,'' mainly MC simulations. The positional correlation functions obtained within the approximate theories like PY, BGY, CHNC, or PC are usually compared with the function evaluated by a MC method [11,12]. Chae and coworkers performed MC simulations for the system of hard disks and tabulated the function $g(r/\sigma)$ for the three reduced packing fractions η/η_{cp}: 0.4, 0.5, and 0.6. Using these results, we calculated the effective magnetic field by numerical integration and the value of the critical coupling K_c from the Weiss magnetic equation of state. The obtained critical points are shown by squares in Fig. 3. At higher fluid densities, they coincide with the critical line predicted by the cell model. We conclude that this theory and the cell model provide only a crude approximation to the critical line in our model of ferromagnetic Ising fluid.

IV. THE CRITICAL EXPONENTS

The magnetic second-order phase transition in the Ising model of a 2D ferromagnetic fluid we studied by varying the temperature at a fixed-particle density. We applied finite-size scaling (FSS) method combined with a single histogram technique [33] to determine the critical behavior of different thermodynamic quantities over the entire critical region. FSS predicts the critical behavior of a system in the thermodynamic limit from the properties of finite systems. The FSS approach to critical phenomena was first proposed by Fisher and Barber [43]. They confirmed the method by existing data on a 2D Ising model, ferromagnetic spherical models, ideal Bose fluids, and real helium films. There have been very extensive and careful studies of critical properties in classical ferromagnetic lattice models by MC simulations combined with FSS and histogram techniques [33–36]. These methods have proven to be very useful also in the studies of phase transitions in ferromagnetic fluids [21,31,32].

In the critical region, there are two important characteristic lengths: the correlation length ξ of the order-parameter fluctuations and the linear size L of the system. The finite-size effects are controlled by a comparison of these lengths. At the critical point, the correlation length ξ diverges and all features on the scale of particle spacing (e.g., the structure or the range of particle interactions) become irrelevant. The determination of the dependence of the spin-correlation length on the temperature and density is thus fundamental in the analysis of magnetic phase transitions [22]. The critical behavior of thermodynamic quantities close to the critical point can be described by a set of critical exponents. The divergence of the correlation length describes the exponent ν. The straightforward method to get this exponent, after location of the critical point via cumulant intersection method, is to inspect the slope $\partial U/\partial K$ of the function $U=f(K)$ at $K=K_c$. The derivative $\partial U/\partial K$ can be obtained by taking finite differences for small enough increments of K. The more accurate and reliable method is, however, to calculate the derivative of the formula (2) with respect to K and to exploit the

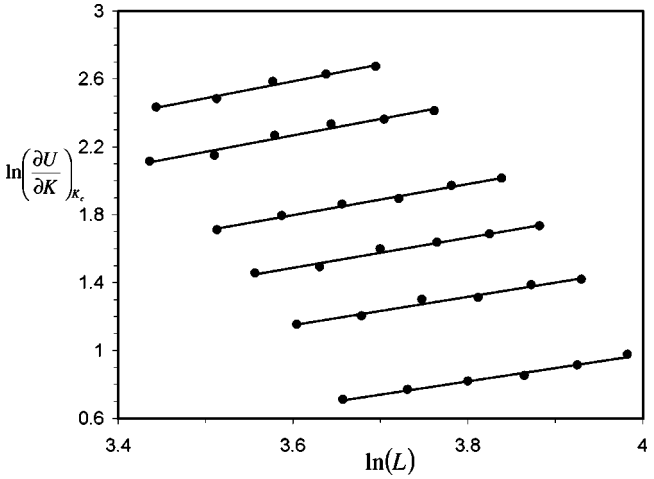

FIG. 4. ln-ln plot of the derivative of the Binder's cumulant at the critical point $(\partial U/\partial K)_{K_c}$ versus the linear system size L. The dots represent data obtained from MC simulations in systems composed of 1296, 1156, 1024, 900, 784, and 676 disks. Every line is the straight line fit to data points corresponding to the same fluid density. The lines are shifted downwards with decreasing density. The slope of these lines gives $1/\nu$, where ν is the correlation length critical exponent. Our estimates of ν for the reduced packing fractions η/η_{cp} equal 0.693, 0.606, 0.520, 0.476, 0.433, and 0.390 are, respectively, 1.00, 1.03, 1.09, 1.13, 1.20, and 1.27. For $\eta/\eta_{cp}=0.693$ the system with 676 disks is omitted.

following equation for the derivatives of the moments of M [21,32,35]:

$$\frac{\partial\langle|M^n|\rangle}{\partial K}=-\frac{1}{K}(\langle|M^n|E\rangle-\langle|M^n|\rangle\langle E\rangle), \tag{4}$$

where $E=0.5\Sigma_{ij}J(r/\sigma)S_iS_j/k_BT$ is the exchange energy of the system divided by thermal energy. The values of averages on the right hand side at $K=K_c$ are determined by applying a single histogram technique. FSS predicts the derivative $(\partial U/\partial K)_{K_c}$ to scale with the system size as $L^{1/\nu}$ [21,28,31,35,36]. In Fig. 4 we show the straight line fits of $\ln(\partial U/\partial K)_{K_c}$ versus $\ln L$ for systems with different densities. The slope of the stright lines is $1/\nu$. The estimated values of the correlation length exponent for different densities are given in this figure. One should notice the increase of ν with decreasing particle density. The independent estimation of the correlation length exponent in ferromagnetic fluids is usually extracted from the critical behavior of derivatives $\partial\ln\langle|M|\rangle/\partial K$ and $\partial\ln\langle M^2\rangle/\partial K$ [32]. These derivatives are expressed in terms of cross correlations with E, and Eq. (4) can be used to calculate them. They have the same scaling properties as the cumulant slope. The maxima of both derivatives are predicted to scale as $L^{1/\nu}$. They are located further from the critical point. At lower fluid densities, positions of the maxima are outside the range of the single histogram generated from the MC run performed near K_c, and we had to make additional MC runs at smaller K values indicated in Table I. The derivatives $\partial\ln\langle|M|\rangle/\partial K$ and $\partial\ln\langle M^2\rangle/\partial K$ allow the estimation of the exponent ν without the knowledge of the critical coupling K_c. In Fig. 5, we plot the logarithm of

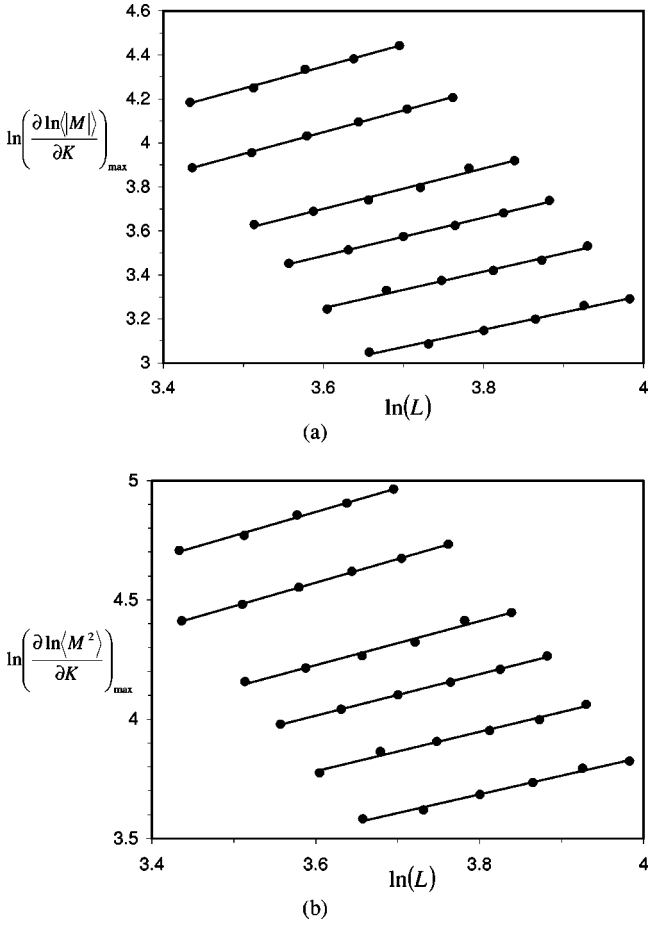

FIG. 5. ln-ln plot of the maximum values of derivatives $\partial\ln\langle|M|\rangle/\partial K$ (a) and $\partial\ln\langle M^2\rangle/\partial K$ (b) versus the linear system size $\ln L$. The dots represent data obtained from MC simulations in systems composed of 1296, 1156, 1024, 900, 784, and 676 disks. Every line is the straight line fit to data points corresponding to the same fluid density. The lines are shifted downwards with decreasing density. The slope of these lines gives $1/\nu$, where ν is the correlation length critical exponent. Our estimates of ν for the reduced packing fractions η/η_{cp} equal 0.693, 0.606, 0.520, 0.476, 0.433, and 0.390, are, respectively, 1.00, 1.01, 1.08, 1.15, 1.20, and 1.27, for the plot (a) and 1.00, 1.01, 1.09, 1.15, 1.21, and 1.28, for the plot (b). For $\eta/\eta_{cp}=0.693$ the system with 676 disks is omitted.

the maximum values of these derivatives versus $\ln L$ and we show values of the exponent ν for different fluid densities estimated from linear fits. These values agree well with values of the exponent ν estimated from the cumulant slope. The dependence of the critical exponent ν on fluid density is given in Table II and shown in Fig. 6. The value $\nu=1.35$ for the number density $\rho=0.4$ ($\eta/\eta_{cp}\simeq0.346$) has been obtained before in Ref. [32]. The continuous variation of the correlation length exponent with fluid density goes against standard universality considerations, but it is qualitatively consistent with the reported variation of ν with the density in Heisenberg fluid [21] and in the 2D site-diluted Ising model [25,29]. Derrida, Southern, and Stauffer [30] suggested that in the system with critical exponents continuously varying with the amount of disorder, the Binder's reduced fourth-order cumulant at the critical point should also vary continu-

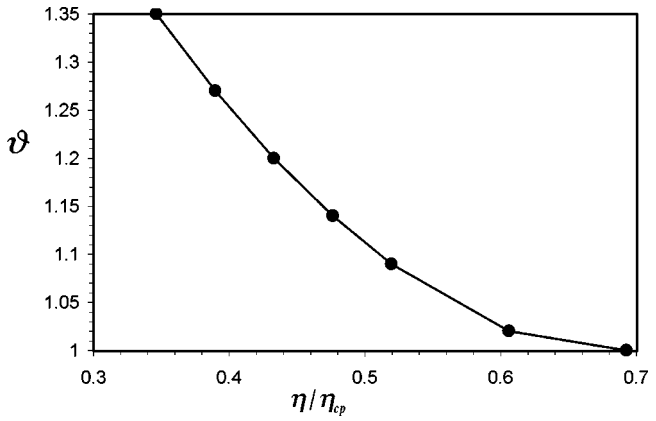

FIG. 6. The correlation length critical exponent ν versus the reduced packing fraction η/η_{cp}. The dots represent values of ν obtained from MC simulations and given in Table II. The curve is drawn to guide the eye.

ously. In Fig. 7, we plot the critical exponent of the spin-correlation length versus the Bindr's fourth-order cumulant at the critical point for different ferromagnetic fluid densities. This dependence is linear, what strongly support the conjecture of Derrida and coworkers.

The basic quantity in the description of phase transitions is the order parameter. For the second-order phase transitions, from the paramagnetic fluid to the ferromagnetic fluid phase, the order parameter is the spontaneous magnetization. It varies continuously across the critical line and it is zero in the paramagnetic phase and nonzero in the ferromagnetic phase. This spontaneous symmetry breaking can occur only in the thermodynamic limit. In MC simulations, the system passes from positive to negative values of M and correct estimates of the spontaneous magnetization have to be defined. The following quantities are often used as estimates of the spontaneous magnetization for MC simulations in finite systems: the peak position of the probability distribution function of M, $\sqrt{\langle M^2\rangle}$ and $\langle|M|\rangle$ [28]. These quantities all tend smoothly towards the spontaneous magnetization in the thermodynamic limit. In this paper, we selected the quantity

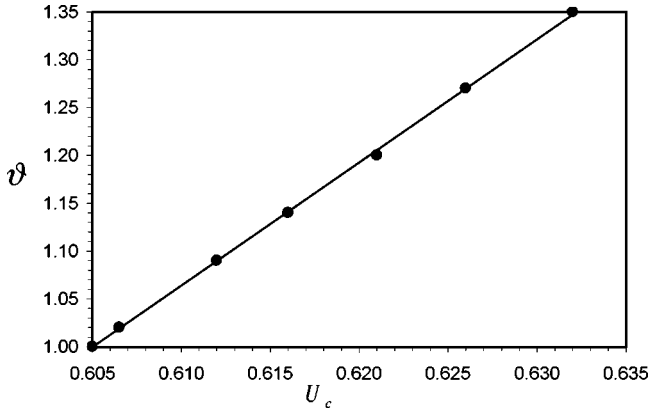

FIG. 7. The correlation length critical exponent ν versus the Binder's cumulant at the critical point U_c. The dots represent data given in Table II that were obtained from MC simulations for different fluid densities. The line is the straight line fit to data points.

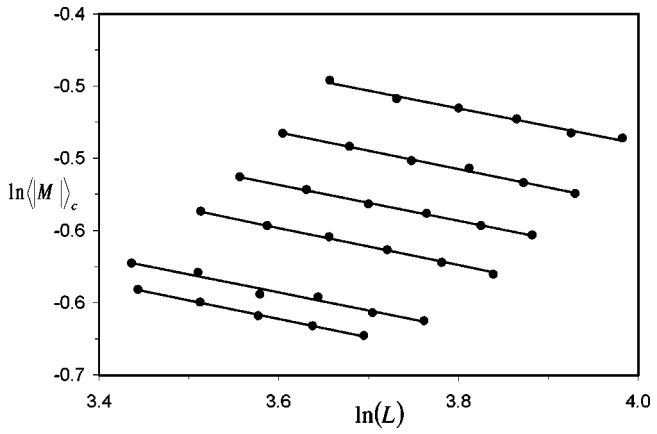

FIG. 8. ln-ln plot of the magnetization at the critical point $\langle|M|\rangle_c$ versus the linear system size L. The dots represent data obtained from MC simulations in systems composed of 1296, 1156, 1024, 900, 784, and 676 disks. Every line is the straight line fit to data points corresponding to the same fluid density. The lines are shifted downwards with increasing density. The slope of these lines equals $-\beta/\nu$. Our estimates of the critical exponent ratio β/ν for the reduced packing fractions η/η_{cp} equal 0.693, 0.606, 0.520, 0.476, 0.433, and 0.390 are, respectively, 0.128, 0.125, 0.128, 0.124, 0.127, and 0.123. For $\eta/\eta_{cp}=0.693$ the system with 676 disks is omitted.

$\langle|M|\rangle$, similar to Refs. [21,32]. The critical behavior of the spontaneous magnetization is described by the exponent β. According to FSS, at the critical point, $\langle|M|\rangle$ varies with the linear system size L as $\langle|M|\rangle_c \simeq L^{-\beta/\nu}$. A straight line fit of $\ln\langle|M|\rangle_c$ versus $\ln L$ gives the exponent ratio β/ν. This is shown in Fig. 8 for different fluid densities. The estimated values of β/ν given in this figure for different reduced packing fractions are all close to the value $\beta/\nu=0.125$, the same as in the 2D Ising lattice model [22]. Although the ratio of exponents β/ν in ferromagnetic fluid is independent of fluid density, both exponents β and ν separately increase with the decreasing of the fluid density. The same qualitative variations of exponents β and ν were reported in Heisenberg ferromagnetic fluid [21], and in the 3D site-diluted Ising lattice model [24].

In the critical region, fluctuations of the order parameter become large and this is expressed by the critical behavior of the magnetic susceptibility χ. The magnetic susceptibility in the thermodynamic limit shows a critical divergence, but in finite systems, it reaches a maximum of finite height. There are various ways to estimate the magnetic susceptibility in finite systems [27,28]. We consider the estimate of the magnetic susceptibility defined as: $\chi=KN(\langle M^2\rangle-\langle|M|\rangle^2)$ [21,32]. The plot of χ versus K in our model presents a very pronounced peak for all fluid densities, similar as in Ref. [32]. The following scaling relations are postulated for the maximum of the susceptibility χ_{max} and for the value of the susceptibility at the critical point χ_c in finite systems [27,28]: $\chi_{\max}\simeq L^{\gamma/\nu}$ and $\chi_c \simeq L^{\gamma/\nu}$. Figure 9 shows and confirms these scaling relations for different fluid densities. The ratio of critical exponents γ/ν is given by the slope of the straight line fit to data in this figure. The obtained values of γ/ν for different fluid densities agree well with the value γ/ν

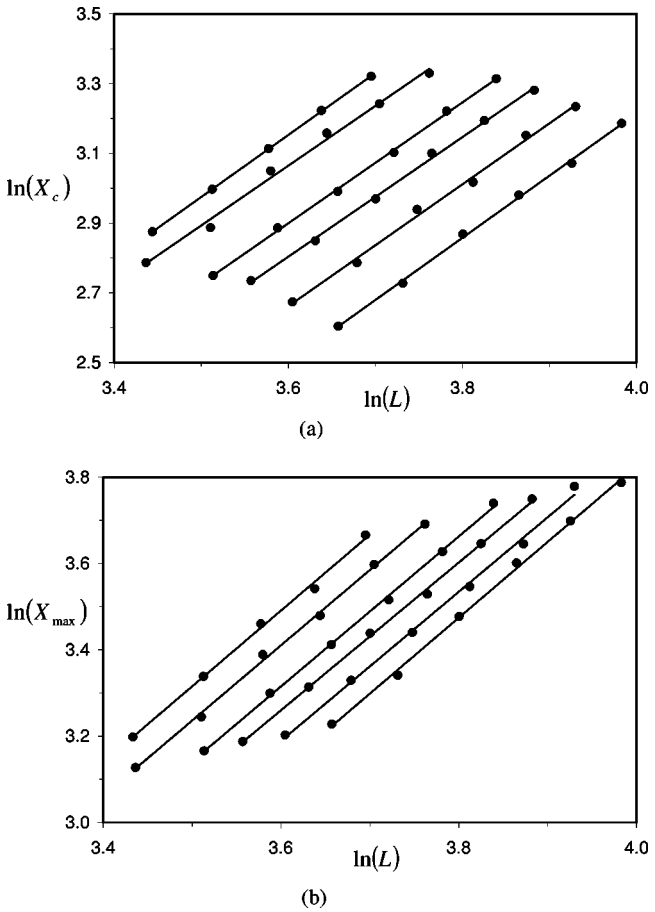

FIG. 9. ln-ln plot of the magnetic susceptibility at the critical point χ_c (a) and at the maximum $\chi_{\max}$ (b) versus the linear system size L. The dots represent data obtained from MC simulations in systems composed of 1296, 1156, 1024, 900, 784, and 676 disks. Every line is the straight line fit to data points corresponding to the same fluid density. The lines shift to the right with decreasing density. The slope of these lines gives the ratio of critical exponents γ/ν. Our estimates of γ/ν for the reduced packing fractions η/η_{cp} equal 0.693, 0.606, 0.520, 0.476, 0.433, and 0.390, are, respectively, 1.78, 1.71, 1.73, 1.72, 1.75, and 1.78, for the plot (a), and 1.76, 1.75, 1.74, 1.71, 1.73, and 1.76, for the plot (b). For $\eta/\eta_{cp}=0.693$ the system with 676 disks is omitted.

$=1.75$ obtained in the 2D Ising lattice model [22]. The ratio γ/ν, independent of the spin density, was also reported in Heisenber fluid [21] and in the 2D site diluted Ising lattice model [25,29].

According to the homogeneity hypothesis, critical exponents of various thermodynamic quantities are related [22]. The relation that connects critical exponents γ, β, and ν has the form: $2\beta/\nu+\gamma/\nu=D$. This relation is satisfied by both the exact and the mean-field critical exponents of the 2D Ising lattice model [22], and by critical exponents determined by several independent methods in the site-diluted 2D Ising lattice model [25,29]. The relation is also satisfied by critical exponents obtained in this paper for all fluid densities, and our results strongly support the validity of the homogeneity hypothesis in ferromagnetic Ising fluid near the second-order phase transition from the paramagnetic to the ferromagnetic fluid phase.

V. ANALYSIS OF THE VORONOI DIAGRAM

The Voronoi diagram in 2D is a straight-line planar graph entirely defined by a given set of points on the plane called generating points. It partitions the plane into regions, which are convex polygons. Each polygon surrounds one generating point and consists of all those points in the plane that are closer to this generating point than to the others. The general properties of Voronoi diagrams in 2D and numerical procedures to generate them are described in Ref. [44]. For systems composed of hard disks, the generating points are the centers of disks. The Voronoi diagrams of the system of hard disks attracted scientific attention some time ago. Smalley [45] proposed to model cooling-induced polygonal crack patterns in lava flows observed in volcanic areas by the Voronoi diagram of the hard-disk system at packing fraction near 0.5. The same model was also used, e.g., to simulate the patterns of receptors in the retina and to describe the fish territories. The more intensive studies of the Voronoi diagram of hard disks at different packing fractions have been done in the last decade. Gervois, Troadec, and Lemaitre [46] studied experimentally hard disks moving on an air cushion table for packing fractions between 0.2 and 0.8. The disks after a short thermalization time form a homogeneous assembly, which may be though of as a 2D particle fluid. The authors took several snapshots of the system at different moments and generated for them Voronoi diagrams. The obtained dependence of the average area of n-sided polygons on n was found to be very different from the Lewis's law observed in many natural cellular structures. They also considered the probability distribution function $P(n)$ of the number of polygon sides n and obtained the universal relation between the variance μ_2 of $P(n)$ and the probability $P(6)$ of the occurrence of hexagons. The experimental system was compared with the hard-disk system generated numerically by the random sequential adsorption (RSA) procedure. In this procedure, disks are sequentially deposited on the plane. The trial position of each disk is chosen at random, and if this position is not rejected due to overlap with already deposited disks, it is accepted and the disk is definitely deposited. This algorithm does not allow any reorganization of particles and only systems with packing fractions up to 0.547 ($\eta/\eta_{cp}\simeq 0.6$) can be built in this way. One should notice that for ($\eta/\eta_{cp}<0.6$) the correlation length critical exponent ν, considered in the previous section, changes with the packing fraction of disks. The work of Gervois, Troadec, and Lemaitre was later extended by Lemaitre and coworkers [47]. The authors determined the probability distribution function of polygon areas and tested the validity of the Aboav-Weaire law in hard-disk systems generated both experimentally and by the RSA numerical procedure. Fraser, Zuckermann, and Mouritsen [2] performed MC simulations of 2D, the hard-disk system in (N,p,T) ensemble in which the particle number N, the pressure p, and the temperature T are fixed [1,37]. The Voronoi diagram was constructed for the initial disk configuration and updated dynamically during the simulation. The authors concentrated on the statistical analysis of Voronoi diagrams for systems of 102 and 408 hard disks at pressures corresponding to reduced packing fractions η/η_{cp} ranging from

0.54 to 0.9. They determined the probability distribution functions for the number of polygon sides and for the polygon side lengths. The second distribution was fitted by the sum of two Gaussians at all densities within the fluid and solid phases. The mean of the Gaussian corresponding to a population of short polygon sides reflects the degree of structural order within the system, and provides a strong signal for the fluid-solid transition in the system. All the above results were obtained for 2D systems composed of noninteracting hard disks.

In this section, we analyze changes of the Voronoi diagram in our ferromagnetic fluid model along the critical line. We performed short MC simulations on systems with 784, 900, 1024, and 1296 particles for densities and K_c values given in Table II. Knowing for each system the average values of the order parameter $\langle |M| \rangle_c$ and the total energy $\langle E \rangle_c$ at the critical point, we stored to a file several configurations for which relative deviations of M and E with respect to these average values were smaller than 0.005. In this way we selected the most typical particle arrangements for the statistical analysis. The examples of such arrangements with their Voronoi diagrams in a system composed of 784 particles at two different densities and $K=K_c$ are shown in Figs. 10 and 11. The Voronoi diagram for the close-packed arrangement of disks consists only of hexagons. As the density is decreased, more and more defects (pentagons and heptagons) appear in the diagram. For densities corresponding to the fluid-solid first-order phase transition, there are disordered domains of ordered disks in the system. The size of these domains decreases, as the system approaches the point of marginal mechanical stability. At lower densities, the arrangement of disks in the system is that of a disordered fluid. The typical structure of the fluid close to the fluid-solid coexistence region is shown in Fig. 10. The topological properties of the Voronoi diagram are usually described by the discrete probability distribution function $P(n)$ of the number of polygon sides n and its moments. This distribution for all obtained typical particle configurations of our systems at the critical point has the maximum at $n=6$. The first moment of $P(n)$ is always six, what follows from Euler's relation and periodic boundary conditions applied to the system. The importance of hexagons in the Voronoi diagram is expressed by two quantities: the second moment μ_2, which describes the dispersion of n around 6 [46,47], and the number of defects $N_{def}=1-P(6)$, which equals to the fraction of polygons with $n\neq 6$ in the diagram [2]. In Fig. 12, we show the dependence of both quantities on fluid density. In this and in the next figures we included the results obtained for densities outside the range of densities given in Table II. For these densities, we assumed values of the critical coupling K_c predicted by the cell model (discussed in the Sec. III) for the screening parameter $z\sigma=\sqrt{2}$. The additional data we determined for systems having the following number densities: $\rho=1.0$ ($\eta/\eta_{cp}\simeq 0.866$, $K_c=0.15$, the initial particle configuration allowed their rearrangement during MC simulations), $\rho=0.9$ ($\eta/\eta_{cp}\simeq 0.779$, $K_c=0.17$), and $\rho=0.38$ ($\eta/\eta_{cp}\simeq 0.329$, $K_c=0.59$). Because they were obtained by performing shorter MC runs, and the solid phase existing at high-disk densities has a structure incommensurate with the square simulation box used [2], points in Figs. 12, 13, and 15 corresponding to the additional data should be treated as approximate results. Both the variance μ_2 and the fractional number of defects N_{def} decrease with increasing the disk density. In the fluid phase, the decrease of μ_2 can be approximated by the straight line. For the reduced packing fraction $\eta/\eta_{cp}=0.55$, the fraction of hexagons in the

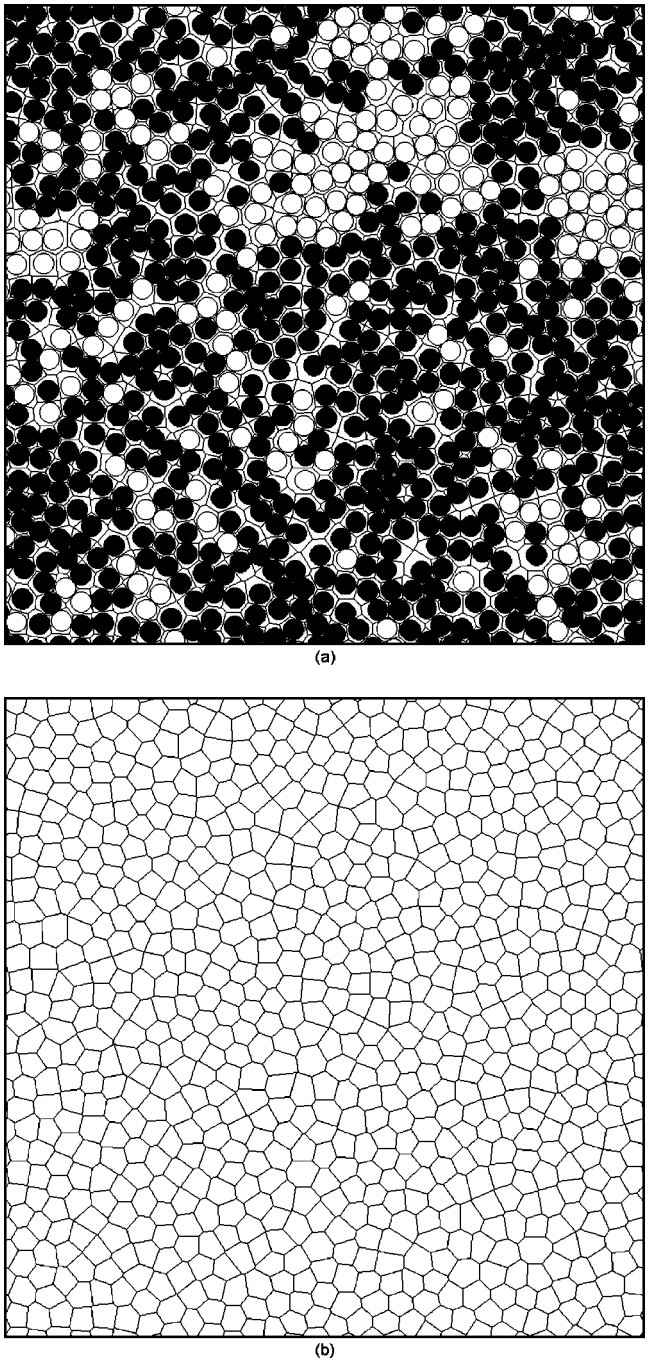

FIG. 10. (a) Typical particle configuration of 2D ferromagnetic Ising fluid at the critical point for the reduced packing fraction $\eta/\eta_{cp}=0.693$, i.e., close to the fluid-solid first-order phase transition, with superimposed Voronoi diagram. The particles with spins up (down) are indicated by black-filled (empty) circles. (b) The Voronoi diagram alone.

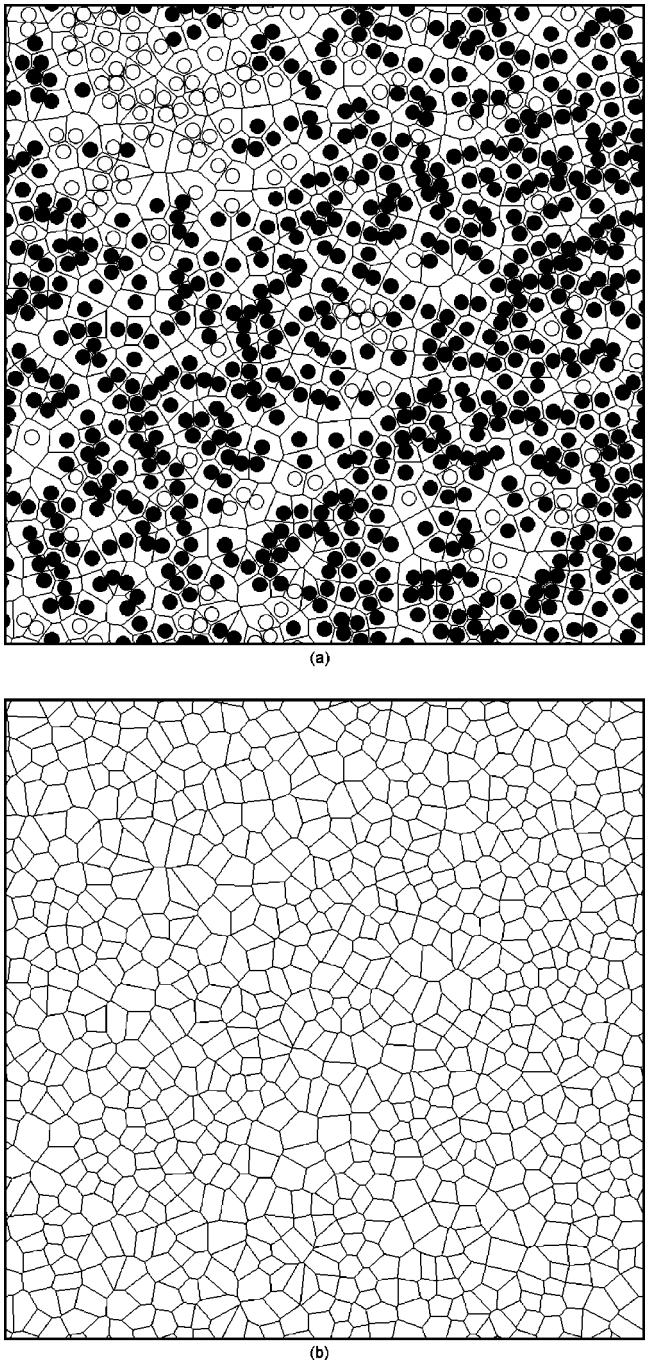

FIG. 11. (a) Typical particle configuration of 2D ferromagnetic Ising fluid at the critical point for the reduced packing fraction $\eta/\eta_{cp}=0.346$, i.e., near the tricritical point, with superimposed Voronoi diagram. The particles with spins up (down) are indicated by black-filled (empty) circles. (b) The Voronoi diagram alone.

Voronoi diagram is the same as other polygons, i.e., $P(6)=N_{def}=0.5$. This density coincides with the lowest density above which the 2D hard-disk system can be described by the free-volume equation of state [3] and critical exponents are similar to those in the 2D Ising lattice model. For $\eta/\eta_{cp}>0.7$, there is a sharp decrease of μ_2 and N_{def}, what is connected with the first-order fluid-solid phase transition and the formation of ordered domains of disks. In this region, $\mu_2=N_{def}$. This universal feature was found in various 2D mosaics at statistical equilibrium for $N_{def}<0.4$ [46,47]. The geometrical properties of the Voronoi diagram of the hard-disk system are usually described by the probability distributions of polygon areas [46,47] or polygon side lengths [2,47]. The second probability distribution was very useful in the description of structural changes in the system of noninteracting hard disks [2]. It was also used to characterize and compare 2D random Voronoi froth (RVF) and random matrix Voronoi froth [48]. RVF is the Voronoi diagram created for points generated by the Poisson point process. RMVF is the 2D Voronoi tessellation with respect to posi-

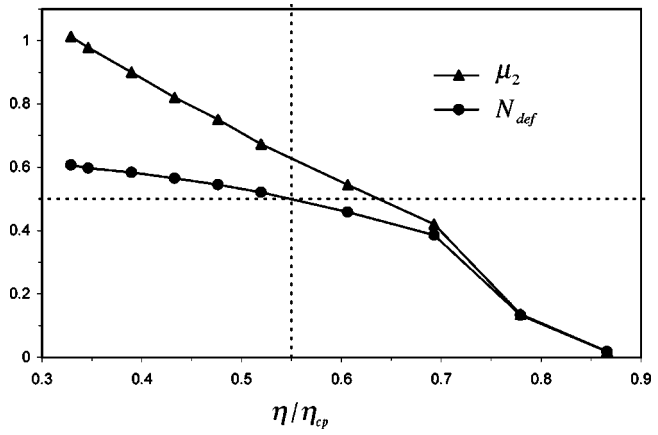

FIG. 12. The fractional number of defects N_{def} and the second moment μ_2 of the probability distribution function of the number of polygon sides in the Voronoi diagram versus the reduced packing fraction η/η_{cp} in 2D ferromagnetic Ising fluid at the critical point. By dotted lines is indicated fluid density for which the fraction of hexagons in the Voronoi diagram is the same as other polygons.

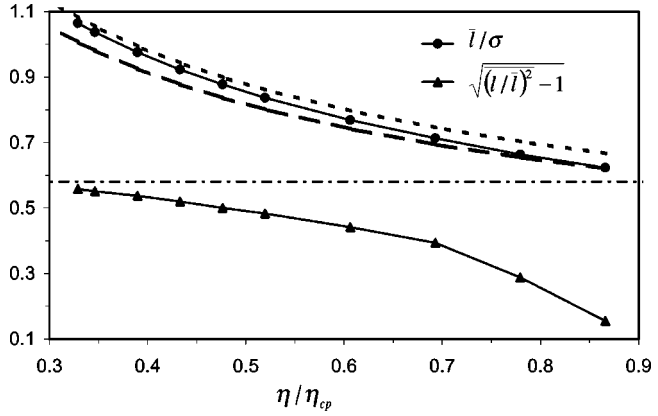

FIG. 13. The dependence of the mean polygon side length normalized by particle diameter $\bar{l}/\sigma$ and the standard deviation for the normalized polygon side lengths $\sqrt{\overline{(l/\bar{l})^2}-1}$ in the Voronoi diagram versus the reduced packing fraction η/η_{cp} for 2D ferromagnetic Ising fluid at the critical point. The dependence of $\bar{l}/\sigma$ on η/η_{cp} for the cell model and for 2D random Voronoi froth is shown by the long-dashed and short-dashed lines, respectively. The dot-dashed line indicates the value $\sqrt{\overline{(l/\bar{l})^2}-1}=0.58$ for the random matrix Voronoi froth.

tions of eigenvalues of asymmetric complex random matrices. The eigenvalues show a repulsion effect characterized by a zero probability of finding two identical eigenvalues. Because of this repulsion, RMVF is more regular than RVF and it resembles the Voronoi diagram of the system of hard disks. We analyzed changes of the Voronoi diagram along the critical line in our model using the probability distribution of polygon side lengths. Let us denote by l the polygon side length. In order to compare probability distributions of l in systems with different densities, we scale polygon side lengths in each system by their mean value $\overline{l}$. Figure 13 shows the dependence of the mean polygon side length normalized by particle diameter $\overline{l}/\sigma$ versus disk density, compared to the dependence $\overline{l}/\sigma=1/\sqrt{3\eta/\eta_{cp}}$ in the cell model with hexagonal cells and to the dependence $\overline{l}/\sigma=1/(1.5\sqrt{\rho})$ derived theoretically for the RVF and used to normalize polygon side lengths in Ref. [48]. It is seen in the approach of $\overline{l}$ to the mean in the cell model at high densities and to the mean in RVF at low densities. In Fig. 13 we also show the dependence of the standard deviation for the normalized polygon side lengths $\sqrt{\overline{(l/\overline{l})^2}-1}$ on disk density. This dependence tends to the value of the standard deviation for the normalized polygon side lengths in RMVF at low densities, and it has a sharp decrease for densities $\eta/\eta_{cp}>0.7$, i.e., above the point of marginal mechanical stability. For each Voronoi diagram, we divided the normalized polygon side lengths $l/\overline{l}$ into bins of size 0.1 and we calculated the discrete probability distribution $P(l/\overline{l})$. The obtained probability distributions $P(l/\overline{l})$ at the critical point in finite systems composed of 1296, 1024, 900, and 784 particles are given in Fig. 14 for the three selected fluid densities. It is seen that probability distributions $P(l/\overline{l})$ in systems with different numbers of particles coincide and they can be fitted by one function. Caër and Ho [48] proposed to fit $P(l/\overline{l})$ by the sum of two Gaussian functions with the same standard deviation and centered symmetrically with respect to $l=0$. This function fits well the distribution $P(l/\overline{l})$ in RVF, but not in RMVF. Fraser and co-workers [2] used the sum of two Gaussians with different means and widths to fit the distribution of Voronoi edge lengths in the system of noninteracting hard disks. The fit was good at all disk densities and the fitting parameters were found to reflect structural properties of the system. In Ref. [2,48] Voronoi diagrams with several dozen polygons were generated and considered. For Voronoi diagrams generated in our systems, we found the best fit of $P(l/\overline{l})$ by the following probability density function:

$$f\left(\frac{l}{\overline{l}}\right)=\sum_{i=1,2}\frac{1}{2\sigma_i\sqrt{2\pi}}\left[\exp\left(-\frac{(l/\overline{l}-m_i)^2}{2\sigma_i^2}\right)+\exp\left(-\frac{(l/\overline{l}+m_i)^2}{2\sigma_i^2}\right)\right], \tag{5}$$

where m_1, m_2, σ_1, and σ_2 are the fit parameters. This function is a sum of two functions having the form given in Ref. [48]. We found it the most reliable and stable for our Voronoi diagrams with several hundred of polygons. The function $P(l/\overline{l})$ well describes the probability density function of polygon side lengths in RVF for $m_1=m_2=0.9144$ and $\sigma_1=\sigma_2=0.7623$, and in RMVF for $m_1=1.3927$, $\sigma_1=0.4587$,

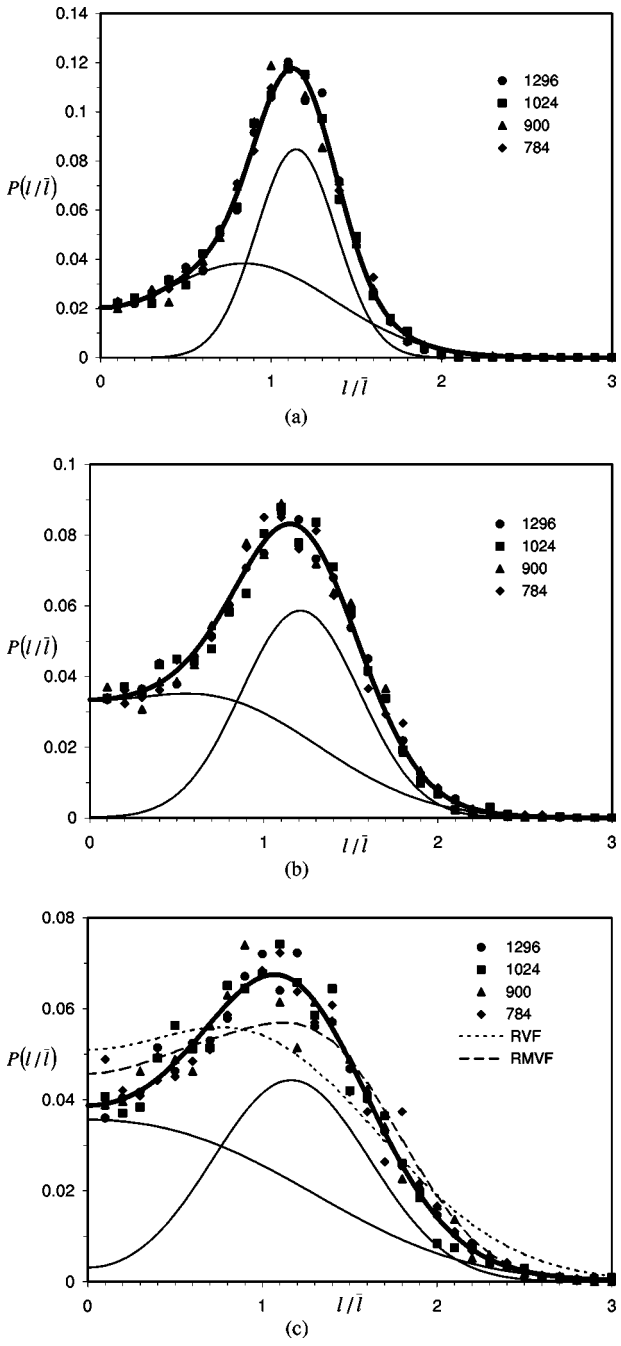

FIG. 14. The probability distributions of normalized polygon side lengths in the Voronoi diagram obtained in systems composed of 1296, 1024, 900, and 784 particles at the critical point for the following reduced packing fractions η/η_{cp}: 0.693 (a), 0.520 (b), and 0.346 (c). The thick solid line is the fit with the probability density function given by Eq. (5). The thin solid lines correspond to two component functions defined in Eq. (5). The probability distributions for random Voronoi froth and random matrix Voronoi froth are shown by the short-dashed and long-dashed lines, respectively.

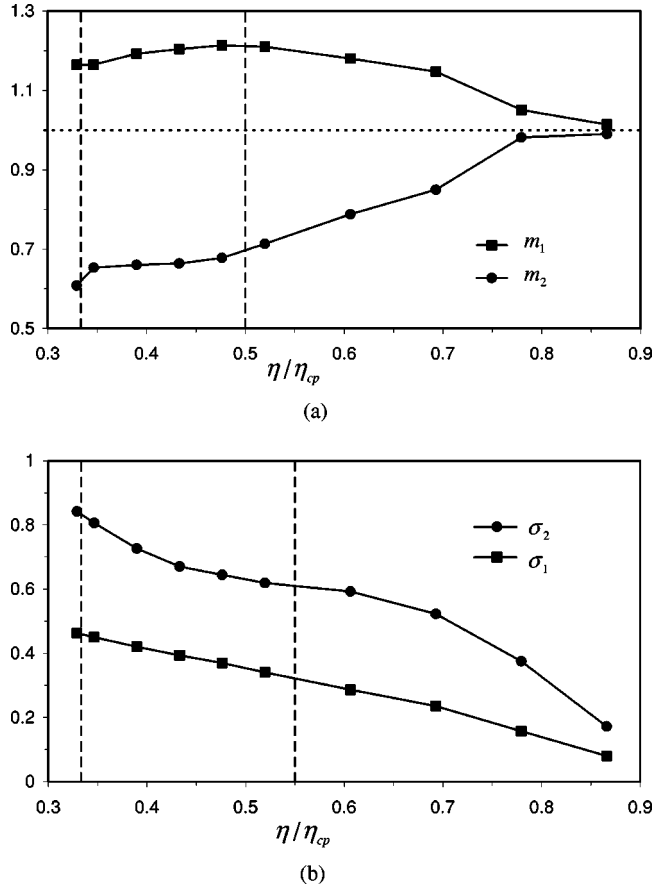

FIG. 15. The fit parameters of the probability density function given by Eq. (5) to the probability distribution of normalized polygon side lengths in the Voronoi diagram generated for 2D ferromagnetic Ising fluid at the critical point, versus the reduced packing fraction η/η_{cp}.

$m_2=0.538$, and $\sigma_2=0.5088$. The probability distributions $P(l/\overline{l})$ for RVF and RMVF are shown by dashed lines in Fig. 14(c). The probability distribution of polygon side lengths in our system for the reduced packing fraction $\eta/\eta_{cp}=0.346$ is closer to the distribution $P(l/\overline{l})$ in RMVF than in RVF. This means that the repulsion of seeds generating the Voronoi diagram in RMVF is still important for the lowest fluid densities considered in this paper. In Fig. 14 we show by thin solid lines the two functions contributing to the probability distribution function $P(l/\overline{l})$ according to Eq. (5). The dependence of their fitting parameters on fluid density is given in Fig. 15. We denoted, similar to Ref. [2], by the subscript 1, the component function that is mainly responsible for the peak in $P(l/\overline{l})$ and by the subscript 2, the second component function that corresponds to the population of short polygon sides. In the solid phase, the Voronoi diagram consists of hexagons with a few defects (pentagons and heptagons). The distribution $P(l/\overline{l})$ is narrow and concentrated around $l/\overline{l}=1$ in this case. In the region of the first-order fluid-solid phase transition, there is a sharp jump in the value of m_2. This can be useful for locating the transition, as it was first proposed by Fraser *et al.* [2] in a system of noninteracting hard disks. As the density of a fluid decreases, the distribution $P(l/\overline{l})$ broadens. The contribution of short polygon sides increases and m_2 moves from 1 to 0.66 for $\eta/\eta_{cp}\simeq 0.346$ ($\rho=0.4$). At lower densities, we observed again sharp decrease of m_2, which signals the approach to the tricritical point. The quantity m_2 can thus be used to characterize the structural order within the system and it is sensitive to structural changes in the system. In the fluid phase, the quantity m_1 is around 1.2 with a small maximum at $\eta/\eta_{cp}\simeq 0.5$. The parameters σ_1 and σ_2 increase with decreasing fluid density. The dependence of σ_1 on the density in the fluid phase is linear, whereas the dependence of σ_2 on the density has the inflexion point. This inflexion point is for $\eta/\eta_{cp}=0.55$, where the fraction of hexagons in the Voronoi diagram is the same as other polygons.

VI. CONCLUSIONS

We described the critical behavior of the 2D ferromagnetic Ising fluid near the second-order phase transition from the paramagnetic fluid to the ferromagnetic fluid phase for densities between the freezing density and the tricritical point density. The description is based on MC simulations combined with finite-size scaling analysis and a single histogram technique. We precisely located the critical line using Binder's reduced fourth-order cumulant, and we determined values of critical exponents ν, β, and γ. We analyzed Voronoi diagrams generated for typical particle configurations along the critical line. We proposed the probability density function with four fit parameters that well describes the distribution of normalized polygon side lengths in Voronoi diagram at all densities. Following are the main conclusions:

(1) The critical exponent of the spin correlation length ν is similar to that in the 2D Ising lattice model for $\eta/\eta_{cp}>0.6$. At lower fluid densities, it increases continuously with decreasing density from 1 to 1.35 in the investigated density range. The ratios of critical exponents γ/ν and β/ν remain the same as in the 2D Ising lattice model at all densities, so the scaling relation $2\beta/\nu+\gamma/\nu=D$ is always satisfied. The results suggest the existence of a line of fixed points with continuously varying critical exponents. This strongly supports the idea of weak universality introduced to describe the similar critical behavior observed in 2D and 3D site-diluted Ising lattice models [24,25,29].

(2) The value of the Binder's reduced fourth-order cumulant at the critical point increases continuously with decreasing fluid density. This was also reported in the 3D Heisenberg fluid [21] and the 2D site-diluted Ising lattice model [25].

(3) There is a liner relation between the critical exponent ν and the value of the Binder's cumulant at the critical point. This supports the conjecture of Derrida *et al.* [30] that the value of the cumulant at the critical point characterizes universality class.

(4) Both the cell model and the theory in which spins are treated in the mean-field approximation and spatial correlations between particles, simillar to those in classical liquids, overestimate the critical temperature. The critical lines predicted by these theories coincide for the reduced packing fraction η/η_{cp} greater than approximately 0.6.

(5) The probability density function describing the distribution of normalized polygon side lengths in Voronoi diagrams generated for typical disk configurations along the critical line can be decomposed into two component functions. The location parameter of one component function can be used to characterize the fluid structure. It signals the approach of the fluid both to the freezing transition and to the tricritical point. This parameter corresponds to the similar parameter defined in Ref. [2].

(6) The fluid density below which the exponent ν varies with density coincides with

• the lowest density above which the 2D hard-disk system can be described by the free-volume equation of state [3],

• the highest density below which the hard-disk system can be generated numerically by the random sequential adsorption algorithm [46],

• the density at which the fraction of hexagons in the Voronoi diagram is the same as other polygons,

• the density at which the scale parameter of one component function of the probability density function describing the distribution of normalized polygon side lengths in Voronoi diagram has the inflexion point.

ACKNOWLEDGMENTS

I thank Raul Toral for discussions and his kind hospitality at Instituto Mediteraneo De Estudios Avanzados (IMEDEA) in Spain, the institute IMEDEA for the grant, and the Department of Physics at the University de les Illes Balears in Spain for the permission to use computers in the Department to perform MC simulations.

[1] J.A. Barker and D. Henderson, Rev. Mod. Phys. **48**, 587 (1976).
[2] D.P. Fraser, M.J. Zuckermann, and O.G. Mouritsen, Phys. Rev. A **42**, 3186 (1990).
[3] N. Metropolis, A.W. Rosenbluth, M.N. Rosenbluth, and A.H. Teller, J. Chem. Phys. **21**, 1087 (1953).
[4] B.J. Alder and T.E. Wainwright, Phys. Rev. **127**, 359 (1962).
[5] W.G. Hoover and B.J. Alder, J. Chem. Phys. **46**, 686 (1967).
[6] W.G. Hoover and F.H. Ree, J. Chem. Phys. **49**, 3609 (1968).
[7] T.V. Ramakrishnan, Phys. Rev. Lett. **48**, 541 (1982).
[8] P. Tarazona, Mol. Phys. **52**, 81 (1984).
[9] J.L. Colot and M. Baus, Phys. Lett. A **119**, 135 (1986).
[10] X.C. Zeng and D.W. Oxtoby, J. Chem. Phys. **93**, 2692 (1990).
[11] F. Lado, J. Chem. Phys. **49**, 3092 (1968).
[12] D.G. Chae, F.H. Ree, and T. Ree, J. Chem. Phys. **50**, 1581 (1969).
[13] G. Busch and H.J. Guentherodt, Phys. Lett. A **27**, 110 (1968).
[14] D. Marx, P. Nielaba, and K. Binder, Phys. Rev. Lett. **67**, 3124 (1991).
[15] D. Marx, P. Nielaba, and K. Binder, Phys. Rev. B **47**, 7788 (1993).
[16] S. Sengupta, D. Marx, and P. Nielaba, Europhys. Lett. **20**, 383 (1992).
[17] N.E. Frankel and C.J. Thompson, J. Phys. C **8**, 3194 (1975).
[18] P.C. Hemmer and D. Imbro, Phys. Rev. A **16**, 380 (1977).
[19] E. Lomba, J.J. Weis, N.G. Almarza, F. Bresme, and G. Stell, Phys. Rev. E **49**, 5169 (1994).
[20] J.M. Tavares, M.M. Telo da Gama, P.I.C. Teixeira, J.J. Weis, and M.J.P. Nijmeijer, Phys. Rev. E **52**, 1915 (1995).
[21] M.J.P. Nijmeijer and J.J. Weis, Phys. Rev. E **53**, 591 (1996).
[22] R. B. Stinchcombe, in *Phase Transitions and Critical Phenomena*, Vol. 7, edited by C. Domb and J. L. Lebowitz (Academic Press, London, 1983), p. 151.
[23] D.P. Landau, Phys. Rev. B **22**, 2450 (1980).
[24] J. Marro, A. Labarta, and J. Tejada, Phys. Rev. B **34**, 347 (1986).
[25] J.K. Kim and A. Patrascioiu, Phys. Rev. Lett. **72**, 2785 (1994).
[26] K. Binder, Phys. Rev. Lett. **47**, 693 (1981).
[27] K. Binder, Z. Phys. B: Condens. Matter **43**, 119 (1981).
[28] K. Binder and D. W. Heermann, *Monte Carlo Simulations in Statistical Physics* (Springer-Verlag, Berlin, 1992).
[29] R. Kühn, Phys. Rev. Lett. **73**, 2268 (1994).
[30] B. Derrida, B.W. Southern, and D. Stauffer, J. Phys. (France) **48**, 335 (1987).
[31] N.B. Wilding and P. Nielaba, Phys. Rev. E **53**, 926 (1996).
[32] A.L. Ferreira and W. Korneta, Phys. Rev. E **57**, 3107 (1998).
[33] A.M. Ferrenberg and R.H. Swendsen, Phys. Rev. Lett. **61**, 2635 (1988).
[34] A.M. Ferrenberg and R.H. Swendsen, Phys. Rev. Lett. **63**, 1195 (1989).
[35] A.M. Ferrenberg and D.P. Landau, Phys. Rev. B **44**, 5081 (1991).
[36] P. Peczak, A.M. Ferrenberg, and D.P. Landau, Phys. Rev. B **43**, 6087 (1991).
[37] M. P. Allen and D. J. Tildesley, *Computer Simulation of Liquids* (Oxford University Press, New York, 1987).
[38] A.M. Ferrenberg, D.P. Landau, and K. Binder, J. Stat. Phys. **63**, 867 (1991).
[39] T.W. Burkhardt and B. Derrida, Phys. Rev. B **32**, 7273 (1985).
[40] J.E. Lennard-Jones, F.R.S. Devonshire, and A.F. Devonshire, Proc. R. Soc. London, Ser. A **163**, 53 (1937).
[41] B.J. Alder, W.G. Hoover, and D.A. Young, J. Chem. Phys. **49**, 3688 (1968).
[42] L. Feijoo, C.W. Woo, and V.T. Rajan, Phys. Rev. B **22**, 2404 (1980).
[43] M.E. Fisher and M.N. Barber, Phys. Rev. Lett. **28**, 1516 (1972).
[44] F. P. Preparata and M. I. Shamos, *Computational Geometry, An Introduction* (Springer-Verlag, Berlin, 1985).
[45] I.J. Smalley, Geol. Mag. **103**, 110 (1966).
[46] A. Gervois, J.P. Troadec, and J. Lemaitre, J. Phys. A **25**, 6169 (1992).
[47] J. Lemaitre, A. Gervois, J.P. Troadec, N. Rivier, M. Ammi, L. Oger, and D. Bideau, Philos. Mag. B **67**, 347 (1993).
[48] G. Le Caër and J.S. Ho, J. Phys. A **23**, 3279 (1990).